REV1-targeting inhibitor JH-RE-06 induces ferroptosis via NCOA4-mediated ferritinophagy in colorectal cancer cells

JIANHUA CHENG[1,2*], XIAOXIA YANG[3*], WEN ZHAO[1], JIE XU[1], YANJIE HAO[1] and FANG XU[1]

[1]School of Basic Medicine, Ningxia Medical University, Yinchuan, Ningxia Hui 750001, P.R. China; [2]Ningxia Key Laboratory of Craniocerebral Diseases, Ningxia Medical University, Yinchuan, Ningxia Hui 750001, P.R. China; [3]Department of Anesthesia and Perioperative Medicine, General Hospital of Ningxia Medical University, Yinchuan, Ningxia Hui 750004, P.R. China

Received May 11, 2025; Accepted August 22, 2025

DOI: 10.3892/or.2025.8992

Abstract. Oncogenes accelerate DNA replication, leading to the activation of excessive replication origins. This process triggers replication stress (RS) and genomic instability in cancer cells, positioning RS as a promising therapeutic target. Translesion synthesis (TLS) functions as a DNA damage repair bypass mechanism, compensating for RS and conferring a proliferation advantage to cancer cells. Despite its therapeutic potential, the application of the TLS polymerase REV1 (REV1 DNA directed polymerase (REV1) inhibitor JH-RE-06 in colorectal cancer (CRC) remains unexplored. Bioinformatics analysis of clinical samples from The Cancer Genome Atlas (TCGA) database demonstrated marked REV1 upregulation in colorectal tumors compared with normal tissues, which was associated with a poorer prognosis. JH-RE-06 effectively suppressed CRC tumorigenesis both *in vitro* and *in vivo*. Mechanistically, drug rescue experiments and proteomics revealed that cell death triggered by JH-RE-06 was associated with elevated oxidative stress and induction of ferroptosis-associated signaling. Transmission electron microscopy revealed characteristic morphological changes associated with ferroptosis, including a significant reduction in mitochondrial abundance and the presence of autophagic vacuoles containing engulfed mitochondria. Biochemical assays confirmed that JH-RE-06 significantly increased intracellular Fe^{2+} and malondialdehyde (MDA) levels while reducing glutathione levels, indicative of ferroptosis. Western blot analysis revealed decreased levels of antioxidant proteins, including superoxide dismutase 2 (SOD2) and glutamate-cysteine ligase catalytic subunit (GCLC), as well as ferritin. Furthermore, western blot and FerroOrange assays, combined with Autophagy-related Gene 7 (ATG7) and Nuclear Receptor Coactivator 4 (NCOA4) knockdown experiments, demonstrated that JH-RE-06 activated ferroptosis in CRC via NCOA4-mediated ferritinophagy. Safety evaluation via hematoxylin and eosin staining of major organs in mice showed no notable pathological damage induced by JH-RE-06. Taken together, these findings establish REV1 as a potential diagnostic biomarker and therapeutic target in CRC. REV1 inhibitor JH-RE-06 promoted NCOA4-mediated ferritinophagy and induced programmed cell death, thereby highlighting its potential as a safe and effective therapeutic strategy for CRC.

Correspondence to: Professor Fang Xu, School of Basic Medicine, Ningxia Medical University, Housheng Building, 1160 Shengli South Street, Yinchuan, Ningxia Hui 750001, P.R. China
E-mail: xufang_1@nxmu.edu.cn

*Contributed equally

Key words: REV1, JH-RE-06, colorectal cancer, NCOA4, ferroptosis

Introduction

Globally, colorectal cancer (CRC) accounted for >1.9 million newly diagnosed cases of cancer in 2020, leading to almost 935,000 fatalities. This accounted for one-tenth of all cancer cases and deaths (1). While chemotherapy is the standard treatment for metastatic CRC, the median overall survival is 20 months (2), and the 5-year survival rate is 12% (3). These statistics reveal the need to unravel the molecular basis of treatment resistance and develop targeted therapies that induce novel forms of programmed cell death (PCD). Although oncogene activation, a hallmark of tumor growth, provides cancer cells with benefits, including resistance to apoptosis and promotion of invasion and metastasis, it also induces replication stress (RS) (4). Cells have evolved multiple mechanisms to manage RS, preventing excess activation that could lead to genomic instability and DNA damage. One such mechanism is specialized translesion synthesis (TLS), which allows DNA replication to proceed past damaged sites, thereby avoiding replication fork failure (5).

In cancer cells, the TLS core factor REV1 (REV1 DNA directed polymerase (REV1) promotes chemotherapy resistance and confers a growth advantage by dynamically recruiting Polζ (B-family DNA polymerase ζ) in an 'on the fly' or 'gap-filling' process. The on the fly process is initiated at platinum-induced DNA damage sites. In this mechanism, the high-fidelity DNA Polδ is functionally replaced by the error-prone TLS polymerase REV1. REV1 inserts a cytosine opposite a lesion or abasic sites, allowing Polζ to continue DNA synthesis before switching back to Polδ. This mechanism

enables cancer cells to bypass the DNA damage and tolerate the toxicity of platinum-based therapy (6-9). The gap-filling process involves temporary single-stranded DNA (ssDNA) gaps resulting from the intermittent synthesis of the lagging strand during DNA replication. In cancer cells, active oncogenes and RS create numerous ssDNA gaps that often require REV1-Polζ for repair, given the fast growth rate of these cells (10,11). Therefore, targeting the REV1-Polζ complex may counteract the development of resistance to platinum-based chemotherapy. Secondly, inhibiting TLS without requiring additional chemotherapy drugs may facilitate the accumulation of ssDNA gaps. These gaps impede the ability of cancer cells to replicate and proliferate (12), ultimately leading to cell death.

REV1 mRNA levels are upregulated 10.3-fold in CRC when DNA mismatch repair is inactivated or p53 is lost (13). The transgenic expression of REV1 in mice accelerates the development of intestinal adenoma, with the rate of development being directly proportional to the levels of REV1 expression (14). A pan-cancer genomic analysis demonstrated an association between low expression of REV1 and a more favorable prognosis for CRC (15). Furthermore, high REV1 expression is associated with a poor prognosis in various types of tumor, including CRC (15). Therefore, small molecule drugs that specifically target REV1 hold promise for CRC treatment.

Research by Wojtaszek *et al* led to the discovery of JH-RE-06, a novel compound targeting REV1 (16). Combining JH-RE-06 with cisplatin arrests tumor growth and significantly prolongs survival in mouse models (16-18), while decreasing cisplatin-induced mutations and enhancing tumor cell sensitivity. Although these findings suggest clinical potential, whether REV1 inhibitors exert unique mechanisms in CRC compared with other cancers remains unexplored. Unlike the senescence-inducing effects of REV1 inhibitors reported in melanoma and ovarian cancer cells (17), JH-RE-06 uniquely triggers NCOA4-mediated ferritinophagy in CRC, which results in increased levels of the labile iron pool (LIP), inducing ferroptosis. N-acetylcysteine (NAC), a cysteine prodrug, effectively rescues this ferroptotic process. While JH-RE-06 does not increase the sensitivity of CRC cells to oxaliplatin (OXA), it effectively suppresses clonal proliferation of OXA-resistant (OXR) cell lines *in vitro* and inhibits the growth of OXR xenograft tumors *in vivo*. As high REV1 expression in CRC tissues is significantly associated with poor patient prognosis (15), the selective inhibition of REV1 by JH-RE-06 to induce ferroptosis offers a potential therapeutic strategy to overcome apoptosis resistance.

Materials and methods

Cell culture. The human CRC cell lines HCT116, SW620 (Wuhan Servicebio Technology Co., Ltd.), and oxaliplatin-resistant HCT116 (OXR-HCT116) (Xiamen Immocell Biotechnology Co., Ltd.) cells were maintained under standard physiological conditions (37˚C, 5% CO_2) using basal DMEM (cat. no. G4511) enriched with 10% FBS (cat. no. G8002) and antibiotic-antimycotic solution (1% v/v; cat. no. G4003; all Wuhan Servicebio Technology Co., Ltd.).

Expression analysis of REV1 in CRC. The paired-end RNA sequencing files from The Cancer Genome Atlas (TCGA, portal.gdc.cancer.gov, accession no. phs000178.v11.p8) for 649 colorectal tumors [colon adenocarcinoma (COAD) n=456, READ n=193; COAD: colon adenocarcinoma; READ: rectal adenocarcinoma) were subjected to quality control. Reads were aligned using STAR (v2.7.10b (19)). Gene expression differences between paired and unpaired datasets were analyzed using R (version 4.2.1, R Foundation for Statistical Computing, r-project.org/). Data visualization was performed with ggplot2 (version 3.4.4, ggplot2.tidyverse.org/), and receiver operating characteristic (ROC) curves were generated using pROC (version 1.18.4, https://cran.r-project.org/package=pROC). Prognostic analysis of gene expression in CRC (GSE17536 and GSE17537) was conducted with PrognoScan (https://dna00.bio.kyutech.ac.jp/PrognoScan/). CRC tissue microarrays (93 tissue cores, 37 paired adjacent non-cancerous and cancer tissue samples, 19 metastatic samples) were obtained from Shanghai Outdo Biotech Co., Ltd (cat. no. T21-1063). Antigen retrieval was performed with 3% H_2O_2 for 10 min at room temperature. Following blocking with 5% normal donkey serum (cat. no. G1217-5ML, Wuhan Servicebio Technology Co., Ltd.) at room temperature for 30 min, tissue sections were probed with REV1-specific primary antibody (cat. no. AB5088; Abcam, 1:250) at 4˚C overnight. Following thorough PBS washing, they were treated with HRP-conjugated donkey anti-goat IgG (cat. no. a0181, Beyotime Institute of Biotechnology; 1:250; room temperature, 45 min) followed by DAB staining (5 min, room temperature). Counterstaining with 0.5% Mayer's hematoxylin was then performed (room temperature, 5 min), after which the sections were dehydrated through graded ethanol, cleared in xylene, and mounted with resin. Stained sections were observed via light microscope (Nikon Eclipse E100). REV1 positive rates were analyzed using ImageJ 1.49v (National Institutes of Health, NIH).

Inhibitors. The following inhibitors were used at 37˚C under 5% CO_2 JH-RE-06 (cat. no. HY-12621; 0.5-5.0 μM, 24 or 72 h treatment; deferoxamine (DFO; cat. no. HY-B1625; 100 or 200 μM, 24 h; Z-VAD-FMK (cat. no. HY-16658B): 5 or 10 μM, 24 h; necrostatin-1 (cat. no. HY-15760): 5 or 10 μM, 24 h; chloroquine (cat. no. HY-17589A): 10 or 20 μM, 24 h; N-acetylcysteine (cat. no. HY-B0215; all MedChemExpress): 15 or 20 mM, 24 h; L-penicillamine (cat. no. 196312; 100 mM, 24 h treatment; and 2-mercaptoethanol (cat. no. M3148; both Sigma-Aldrich; Merck KGaA): 2 mM, 24 h treatment.

RNA interference. Transfection was performed when $2x10^5$ HCT116 cells in the six-well plate reached 60% confluency. For liposomal transfection complex formation, 15 μl Lipofectamine™ 3000 (cat. no. L3000001, Thermo Fisher Scientific, Inc.) was mixed with 250 μl Opti-MEM™ reduced serum medium (cat. no. 31985070, Gibco) and incubated at room temperature for 5 min. A total of 15 μl small interfering (si) RNA [ATG7 (Autophagy-related gene 7) RNA I (cat. no. 6604, Cell Signaling Technology, Inc., sequences not available), NCOA4-targeting and scramble siRNA (sequences provided in Table I; Tsingke Biotechnology Co., Ltd.)] at a final concentration of 50 nM was separately diluted in 250 μl Opti-MEM reduced serum medium. Each siRNA diluent was mixed with the Lipofectamine™ 3000-Opti-MEM™ mixture, and the transfection complexes were incubated at

Table I. RNA interference sequences.

Target Gene	Primer Name	Sense Sequence (5'→3')	Antisense Sequence (5'→3')
NCOA4	NCOA4-01	GACCUUAUUUAUCAGCUUA	UAAGCUGAUAAAUAAGGUC
	NCOA4-02	GGAGAACAGUCAGACUUCU	AGAAGUCUGACUGUUCUCC
	NCOA4-03	CCAGGAAGUAUUACUUAAU	AUUAAGUAAUACUUCCUGG
Negative control	Scramble	CUAGAUACUAGACUGAUAA	UUAUCAUCUAGUUAUCUAG

NCOA4, nuclear receptor coactivator 4.

room temperature for 20 min. The cells were cultured at 37˚C under 5% CO_2 for 48 h. followed by western blot analysis to determine the knockdown efficiency of ATG7 and NCOA4.

Tandem mass tags (TMT) proteomic sequencing. A total of 5x10^5 HCT116 cells underwent treatment with DMSO or 3 μM JH-RE-06 for 24 h prior to washing with PBS and cell harvesting at room temperature. Following centrifugation at 15,000 g, 4˚C for 30 h, the soluble protein fraction was isolated, and underwent BCA protein quantification assay. Following concentration normalization (BCA assay: 2 μl diluted sample/BSA standard in 96-well plate, 200 μl 50:1 Buffer A/B at 37˚C for 30 min, absorbance 562 nm to calculate concentration; adjusted to uniform level with PBS), samples underwent tryptic digestion (37˚C, overnight), followed by lyophilization and storage at -80˚C. TMTpro reagents (cat. no. a52047, Thermo Fisher Scientific, Inc.) were used for peptide labeling, followed by reverse-phase chromatographic separation. Agilent 1100 HPLC with Zorbax Extend-C18 column was used: mobile phases A (2:98 ACN-H_2O, pH 10) and B (90:10 ACN-H_2O, pH 10), 300 μl/min, 210 nm detection. Eluates (8-54 min) collected cyclically into tubes, lyophilized, frozen for MS. The samples were loaded onto an Acclaim PepMap RSLC column (75 μm x50 cm, RP-C18, Thermo Fisher) for separation at a flow rate of 300 nl/min. Data were analyzed using Proteome discoverer 2.4.1.15 (Thermo Fisher Scientific). Pathway analysis of differentially expressed proteins was performed using the KEGG (Kyoto Encyclopedia of Genes and Genomes) database (integrated with KEGG annotation results). The hypergeometric distribution test was applied to calculate the significance of differential protein enrichment in each pathway entry, which was represented by the P-value.

Western blotting. A total of 5x10^5 HCT116 or SW620 cellular proteins were extracted using RIPA buffer (cat. no. p0013b, Beyotime Institute of Biotechnology). Protein concentration was determined using the BCA assay. A total of 30 μg of protein per lane was resolved via 12% SDS-PAGE and electroblotted onto PVDF membranes (200 mA, 90 min). Following blocking with 5% skimmed milk at room temperature for 1 h, membranes were probed with primary antibodies (4˚C, overnight) and corresponding secondary antibodies (1:1,000 dilution, cat. no. zb-2301 for anti-rabbit; cat. no. zb-2305 for anti-mouse, Beijing Zhongshan Jinqiao Biotechnology Co., Ltd.) conjugated to horseradish peroxidase at room temperature for 90 min, followed visualization using an ECL kit (cat. no. s6009l, Ue landy). Densitometric analysis was performed using ImageJ 1.49v (National Institutes of Health). The primary antibodies were as follows: Glutathione peroxidase 4 (GPX4; cat. no. 52455), NCOA4 (Nuclear receptor coactivator 4, cat. no. 66849), FTH1 (Ferritin heavy chain 1, cat. no. 3998), γH2AX (Phosphorylated histone H2AX, cat. no. 2577), SOD2 (Superoxide dismutase 2, cat. no. 13141), H2AX (cat. no. 2595), and ATG7 (cat. no. 2631; all 1:1,000, Cell Signaling Technology, Inc.). FTL1 (ferritin light chain 1, cat. no. 84731-7-RR), GCLC (Glutamate-cysteine ligase catalytic subunit, cat. no. 12601-1-AP; both Proteintech Group, Inc.), LC3I/II (Microtubule-associated protein 1 light chain 3 I/II, cat. no. 14600-1-AP), p62 (Sequestosome 1, cat. no. 66184-1-Ig), Tubulin (cat. no. 11224-1-AP), and GAPDH (all 1:2,000, cat. no. 60004-1-Ig, Proteintech Group, Inc.).

Transmission electron microscopy (TEM). 5x10^5 HCT116 or SW620 cells treated with JH-RE-06 (1.5 and 3.0 μM for HCT116 cells, and 1.0 and 1.5 μM for SW620 cells), or 9 μl DMSO at 37˚C for 24 h, then collected and fixed overnight at 4˚C in a fixation solution (cat. no. G1102; Wuhan Servicebio Technology Co., Ltd.). This was followed by 2 h fixation at room temperature using 1% osmium tetroxide in PBS. Following washing by PBS, samples underwent gradient dehydration using ethanol and acetone. Samples were embedded in 812 embedding agent (cat. no. GP2001, Wuhan Servicebio Technology Co., Ltd.) and acetone. Embedding was performed overnight at 37˚C, followed by polymerization at 60˚C for 48 h. Ultrathin sections (60 nm) were dual-stained: uranyl acetate (5% aqueous solution) at 37˚C for 15 min, followed by lead citrate (0.5% aqueous solution) at room temperature for 15 min, then air-dried and imaged using a Hitachi HT7700 TE microscope. Mitochondrial numbers were counted, and autophagic vacuoles with engulfed mitochondria were analyzed using ImageJ 1.49v (National Institutes of Health).

Immunofluorescence assay. HCT116 cells were fixed with 4% PFA for 15 min at room temperature. Subsequently, 0.5% Triton X-100 was applied for 20 min for permeabilization at room temperature. Finally, non-specific binding sites were blocked with 10% goat serum (cat. no. C0265, Beyotime Institute of Biotechnology) for 30 min at room temperature. Following blocking, cells were incubated with γH2AX primary antibody (cat. no. 2577, Cell Signaling Technology, 1:500) at 4˚C for 16 h, then exposed to fluorescent secondary antibody (Alexa-Fluor 488; cat. no. ab150077, Abcam; 1:1,000)

for 1 h at room temperature in the dark and finally stained with DAPI using a 1 μg/ml aqueous solution at room temperature for 5 min for nuclear visualization. Samples were mounted with antifade medium (cat. no. P0128S, Beyotime) and imaged by confocal microscopy, and image analysis was performed using NIS-elements viewer 5.21 (Nikon Instruments, Inc.).

Cell Counting Kit (CCK)-8 assay. HCT116 or SW620 cells in the logarithmic growth phase were trypsinized, resuspended in complete DMEM ($5x10^3$ cells/100 μl) and seeded into 96-well plates (100 μl/well). Following 24 h culture at 37˚C, the medium was replaced with medium containing JH-RE-06 (0.0, 0.5, 1.0, 1.5, 3.0, 5.0 μM), and cells were cultured at 37˚C for 24 or 72 h. CCK-8 reagent (cat. no. C6005, Us Everbright Inc.) was added (1 h, 37˚C in the dark), and the absorbance was measured at 450 nm.

Clone formation assay. Following 50 μM OXA or 3.0 μM JH-RE-06 treatment (24 h, 37˚C), OXR-HCT116 cells were resuspended in DMEM following trypsin digestion to prepare a cell suspension; subsequent cell counting was performed, and the cells were then diluted to the same density using DMEM. After being plated (1,000, 2,000 and 5,000 cells/well) in 6-well plates and maintained at 37˚C for 14 days, the cultured cells were fixed with 4% paraformaldehyde solution for 20 min at room temperature, with subsequent PBS washing. Cells were stained with 0.2% crystal violet for 5 min at room temperature. Under a light microscope, positive clones (defined as cell aggregates containing >50 cells) were identified and counted manually. Then the cloning rate was determined by dividing the clone count by the initial number of seeded cells.

Ferroptosis assay. $5x10^5$ HCT116 cells were treated with 3.0 μM JH-RE-06, and $5x10^5$ SW620 cells were treated with 1.5 μM JH-RE-06 at 37˚C for 6, 12 and 24 h, respectively. A assay kits were used to measure Fe^{2+} content (Cell Ferrous Iron Colorimetric Assay kit; cat. no. E-BC-K881-M, Wuhan Elabscience Biotechnology Co., Ltd.), malondialdehyde (MDA) levels (MDA Detection kit; cat. no. KGT003) and glutathione (GSH) content (GSH Detection kit; cat. no. KGT006, both Jiangsu Kaiji Biotechnology Co., Ltd.) according to the manufacturers' instructions. Following 3.0 μM JH-RE-06 treatment (24 h, 37˚C), $5x10^5$ HCT116 cells were washed with PBS and incubated with FerroOrange fluorescent probe (cat. no. F374, Dojindo Laboratories Inc.; 1 μmol/l working concentration) at 37˚C for 30 min. Cells were washed again with PBS and imaged using laser confocal microscopy and image analysis was performed using NIS-Elements Viewer 5.21.

Animal experiment. 24 Male BALB/c nude mice (age: 4-5 weeks; initial weight: 18-22 g; Ningxia Medical University Laboratory Animal Center) were housed at 25˚C, relative humidity at 50%, a 12 h light/12 h dark cycle, and ad libitum access to sterile standard rodent chow and filtered water. All methods received approval from the Laboratory Animal Ethical and Welfare Committee at Ningxia Medical University Laboratory Animal Center (approval no. IACUC-NYLAC-2022-022). Each mouse was injected with $5x10^6$ OXR-HCT116 cells into the axilla. After 12 days of post-injection culture, the mice were randomized into three groups (n=8 per group based on power analysis) as follows: i) Oxaliplatin (5 mg/kg, i.p.), ii) JH-RE-06 (1.6 mg/kg, intratumoral) and iii) DMSO (100 μl, intratumoral), all of which were administered every 48 h to monitor therapeutic effects and recovery. The maximum volume of the tumor was <2,000 mm^3 (volume=π/6x length x width x height). The maximum tumor volume and diameter were 1,450 mm^3 and 15 mm, respectively. Following 20 consecutive administrations, animals were euthanized with isoflurane, perfused with PBS and 4% paraformaldehyde at room temperature (15 min) and organs (heart, liver, spleen, lung and kidney) and tumor samples were collected and measured. Anesthesia for all surgical and tumor measurement procedures consisted of isoflurane (5% for induction, 2% for maintenance). Confirmation of death was established by the absence of a pedal/toe pinch reflex and the cessation of breathing for ≥1 min.

Immunohistochemistry. Paraffin-embedded tumor specimens were prepared by fixing tissues with 4% paraformaldehyde (4˚C, 12 h), embedding in paraffin, and sectioning into 5 μm-thick slices. Sections were deparaffinized (xylene/ethanol) and subjected to EDTA-mediated antigen retrieval (0.01 M EDTA, pH 9.0; 95˚C, 5 min). Endogenous peroxidase was quenched with 3% H_2O_2 (room temperature, 10 min). Non-specific binding was blocked with 10% goat serum (cat. no. C0265, Beyotime; room temperature, 30 min). Sections were probed with anti-PCNA (cat. no. GB11010-50, Wuhan Elabscience Biotechnology Co., Ltd.; 1:500) and Ki-67 (cat. no. GB111499-100, Wuhan Elabscience Biotechnology Co., Ltd.; 1:200) antibodies (4˚C, overnight). Following PBS-T (0.05% Tween-20) washes, they were treated with HRP-conjugated goat anti-rabbit IgG (cat. no. G1213-100UL, Wuhan Elabscience Biotechnology Co., Ltd.; 1:200; room temperature, 45 min), followed by DAB chromogen staining (5 min). Then counterstaining with 0.5% Mayer's hematoxylin (room temperature, 5 min) and mounting. Stained sections were observed via light microscope (50 μm scale bar; Nikon Eclipse E100). PCNA/Ki-67 positive rates were analyzed using ImageJ 1.49v (National Institutes of Health).

H&E staining. Mouse organ wax blocks were sequentially deparaffinized in graded xylene (analytical grade) and dehydrated in a series of ethanol (70%→80%→95%→100%, v/v). Hematoxylin staining (working concentration: 0.5%, w/v; cat. no. Y269827, Beyotime) was performed at room temperature for 5 min, followed by tap water washing. Differentiation and eosin counterstaining (working concentration: 0.5%, w/v; cat. no. C0109, Beyotime Institute of Biotechnology) were conducted at room temperature for 3 min. After re-dehydration in the above ethanol gradient and clearing in xylene (analytical grade, room temperature), sections were mounted with neutral gum and examined under a light microscope (Nikon Eclipse E100).

Reactive oxygen species (ROS) detection. $5x10^5$ HCT116 cells were treated with 3.0 μM JH-RE-06 for at 37˚C for 24 h. Then, the cells were loaded with 10 μM DCFH-DA (dissolved in serum-free DMEM medium) and incubated at 37˚C for 30 min in the dark. Subsequently, cells were washed 3 times

with pre-warmed (37˚C) PBS. ROS-derived green fluorescence (488/525 nm) was imaged using a inverted fluorescence microscope. Image acquisition and fluorescence intensity quantification were conducted using NIS-Elements Viewer 5.21. ROS levels were calculated as the mean fluorescence intensity of cells in the captured fields.

Statistical analysis. The experiments were repeated in triplicate. All data are presented as mean ± standard error of the mean (SEM). Statistical analysis was performed using GraphPad Prism 9.5.1 (Dotmatics, Inc.), employing one-way ANOVA followed by Sidak's post hoc test. Paired comparisons were performed by Wilcoxon signed-rank test. $P<0.05$ was considered to indicate a statistically significant difference.

Results

REV1 is upregulated in CRC tissue and associated with a poor prognosis. To delineate the role of REV1 in colorectal carcinogenesis, the present study assessed transcriptomic profiles from 644 TCGA colorectal adenocarcinoma samples (COAD/READ). Ggplot2-based analysis demonstrated significantly elevated expression of both REV1 and REV7 in tumor vs. adjacent normal tissue, consistent across unpaired (Fig. 1A) and paired sample analyses (Fig. 1B). The baseline characteristics of the patients are provided in Table SI. Expression levels were not significantly associated with clinicopathological parameters, including sex, age, TNM stage, or perineural invasion. Conversely, the presence of colon polyps was associated with REV1. Significant differences were found in lymphatic invasion with respect to REV1 expression (Table SI). The PrognoScan database was used to assess the association between REV1 expression and CRC prognosis (20). Analysis of datasets GSE17536 and GSE17537 showed a significant association between high REV1 expression and poor prognosis (Fig. 1C). To detect the expression of REV1, quantitative IHC analysis was performed on 35 paired specimens using tissue microarrays (Baseline information for CRC tissue chips is provided in Table SII). Consistent with TCGA findings, there was a significant increase in REV1 protein levels in CRC tumors compared with the paired normal tissues (Fig. 1D and E). Overall, these findings established high REV1 expression as a negative prognostic marker in CRC.

REV1 inhibitor JH-RE-06 suppresses CRC tumorigenesis both in vitro and in vivo. To exploit REV1 as a drug target, the present study evaluated JH-RE-06, a compound that impairs REV1 function by inducing inactive dimer formation (16). CCK-8 assay revealed that JH-RE-06 decreased the proliferation of CRC cells in a dose- and time-dependent manner and induced DNA damage, as indicated by increased γH_2AX levels (Fig. 2A). While JH-RE-06 is hypothesized to enhance tumor cell sensitivity to platinum-based drugs (21), western blot and immunofluorescence analysis show that JH-RE-06 did not modify the effect of OXA in HCT116 cells (Fig. 2B and C). To assess its efficacy in resistant models, OXR-HCT116 cells were used (Fig. S1A). Crystal violet staining demonstrated that JH-RE-06 effectively inhibited the clonogenic capacity of OXR-HCT116 cells (Fig. S1B). Therapeutic efficacy of JH-RE-06 was assessed *in vivo* using a xenograft mouse model developed with OXR-HCT116 cells (Fig. S1C). The JH-RE-06 group displayed a substantial reduction in tumor volume, indicating its effectiveness against OXR malignancies (Figs. 2D and S1D). Safety of JH-RE-06 was assessed by hematoxylin and eosin staining of the hearts, livers, spleens, lung and kidney of treated mice. No notable pathological damage was observed in these major organs (Fig. S1E). Immunohistochemistry for proliferation markers Ki67 and PCNA revealed that JH-RE-06 significantly suppressed tumor growth and blood vessel formation (Fig. 2E). In summary, the REV1 inhibitor JH-RE-06 induced DNA damage in CRC cells and inhibited tumor growth both *in vitro* and *in vivo*.

Cell death induced by REV1 inhibition is associated with oxidative stress and ferroptosis. To investigate the mechanism by which JH-RE-06 causes cell death, CRC cells were pre-treated with inhibitors that target different PCD pathways, such as apoptosis (Z-VAD-FMK), necroptosis (necrostatin-1), autophagy (chloroquine), ferroptosis [deferoxamine, DFO), and antioxidants (L-penicillamine, 2-mercaptoethanol, and N-acetylcysteine). CCK-8 assay showed that DFO partially alleviated JH-RE-06-induced cell death, while antioxidants almost completely reversed this in both HCT116 and SW620 cells (Fig. 3A and B). To investigate global proteomic changes, TMT proteomics was performed on HCT116 cells treated with DMSO or 3 μM JH-RE-06 for 24 h. Proteomic analysis revealed 650 significantly altered proteins following JH-RE-06 treatment (Fig. 3C). Downregulated proteins were predominantly enriched in 'DNA replication', 'oxidative phosphorylation', and 'cell cycle' (Fig. 3D). Notably, a subset of these downregulated proteins was also associated with mitochondrial function, including mitochondrial ribosomal protein small and large subunits and members of the NADH:ubiquinone oxidoreductase subunit family (Fig. 3F). Upregulated proteins were significantly associated with 'ferroptosis' and oxidative stress pathways, including 'steroid biosynthesis', 'cysteine and methionine metabolism', and 'citrate cycle (TCA cycle)' (Fig. 3E). These findings suggested that REV1 inhibition modulated oxidative stress, mitochondrial function and ferroptosis.

JH-RE-06 triggers ferroptosis in CRC cells. Ferroptosis is characterized by iron-catalyzed lipid peroxidation and is controlled by mitochondrial activity and LIP concentrations. Therefore, the present study investigated the subcellular changes in JH-RE-06-treated CRC cells. TEM revealed a significant reduction in mitochondrial abundance in both HCT116 and SW620 cells after 24 h JH-RE-06 treatment (Fig. 4A and B). Autophagic vacuoles containing engulfed mitochondria were observed (Fig. 4A and B). Intracellular free Fe^{2+} levels increased following 6 h treatment, peaking at 24 h in both HCT116 and SW620 cells (Fig. 4C and D). Concurrently, levels of the lipid oxidation marker MDA and ROS increased, while GSH levels decreased over time (Figs. 4C and D and S2A). These results collectively indicated that JH-RE-06 induced a time-dependent increase in Fe^{2+} and MDA levels, alongside a decrease in GSH levels. Furthermore, western blot analysis confirmed that the protein expression levels of mitochondrial (SOD2) and ferritin-(FTL) and glutathione-related proteins (GCLC) decreased following treatment

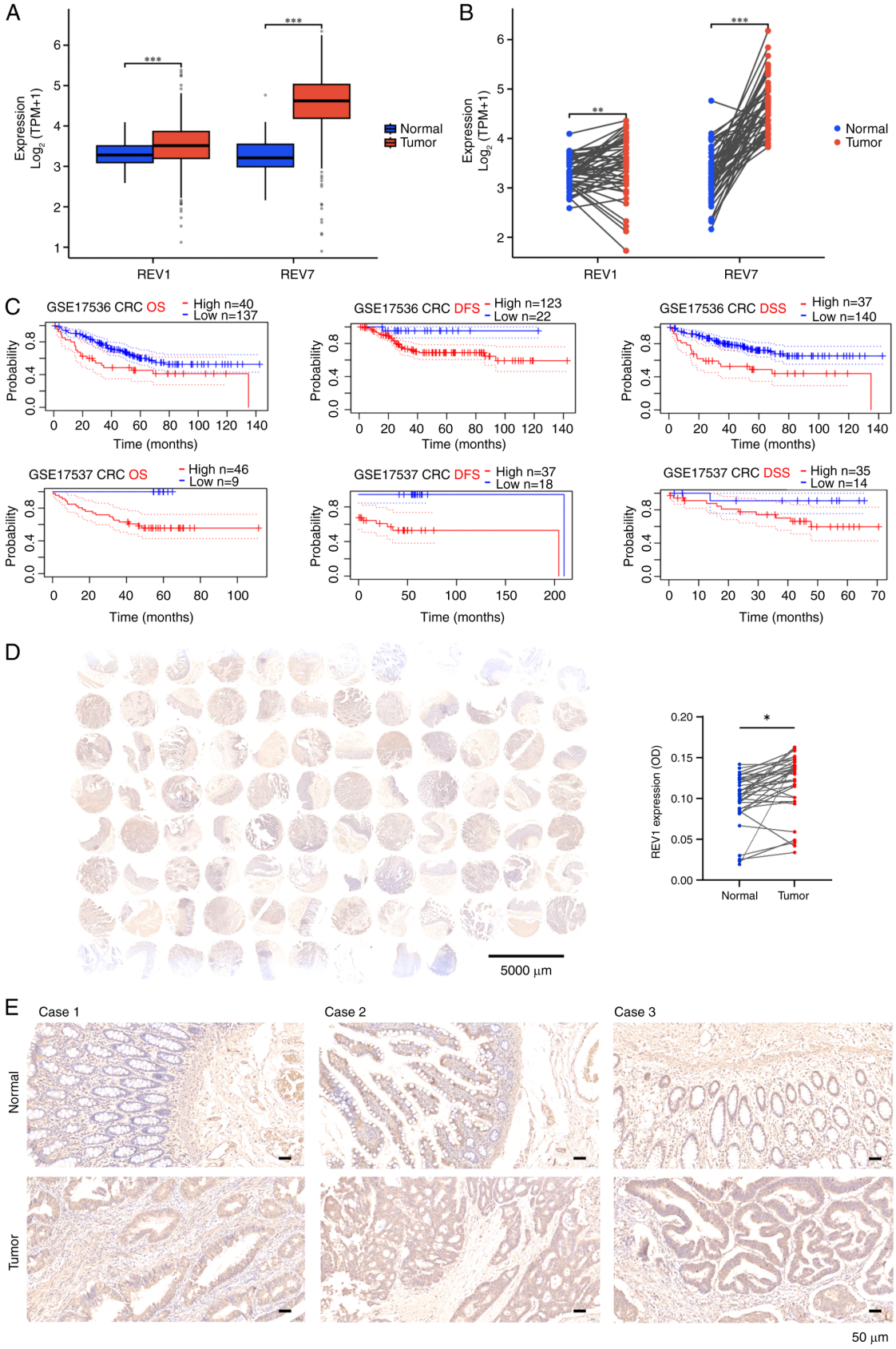

Figure 1. REV1 expression is upregulated in CRC tissues and associated with poor prognosis. (A) Analysis of 644 unpaired samples from TCGA database revealed elevated expression of the REV1 and its binding partner REV7 in clinical CRC samples. (B) Analysis of 50 paired samples from TCGA database showed that REV1 and REV7 were significantly more highly expressed in cancer compared with adjacent non-cancerous tissue. (C) Prognostic analysis of REV1 in CRC was performed using PrognoScan database datasets (accession no. GSE17536/37). (D) REV1 expression levels were analyzed in 35 paired CRC tissue samples using a tissue microarray, which revealed significantly elevated REV1 expression in CRC vs. adjacent normal tissue. (E) Representative immunohistochemical REV1 staining in CRC tissue. Scale bar, 50 μm. ***P<0.001, **P<0.01, *P<0.05. REV1, REV1 DNA directed polymerase; CRC, colorectal cancer; TCGA, The Cancer Genome Atlas; TPM, transcripts per kilobase of exon model per million mapped reads; DFS, disease-free survival; OS, overall survival; DSS, disease-specific survival; OD, optical density.

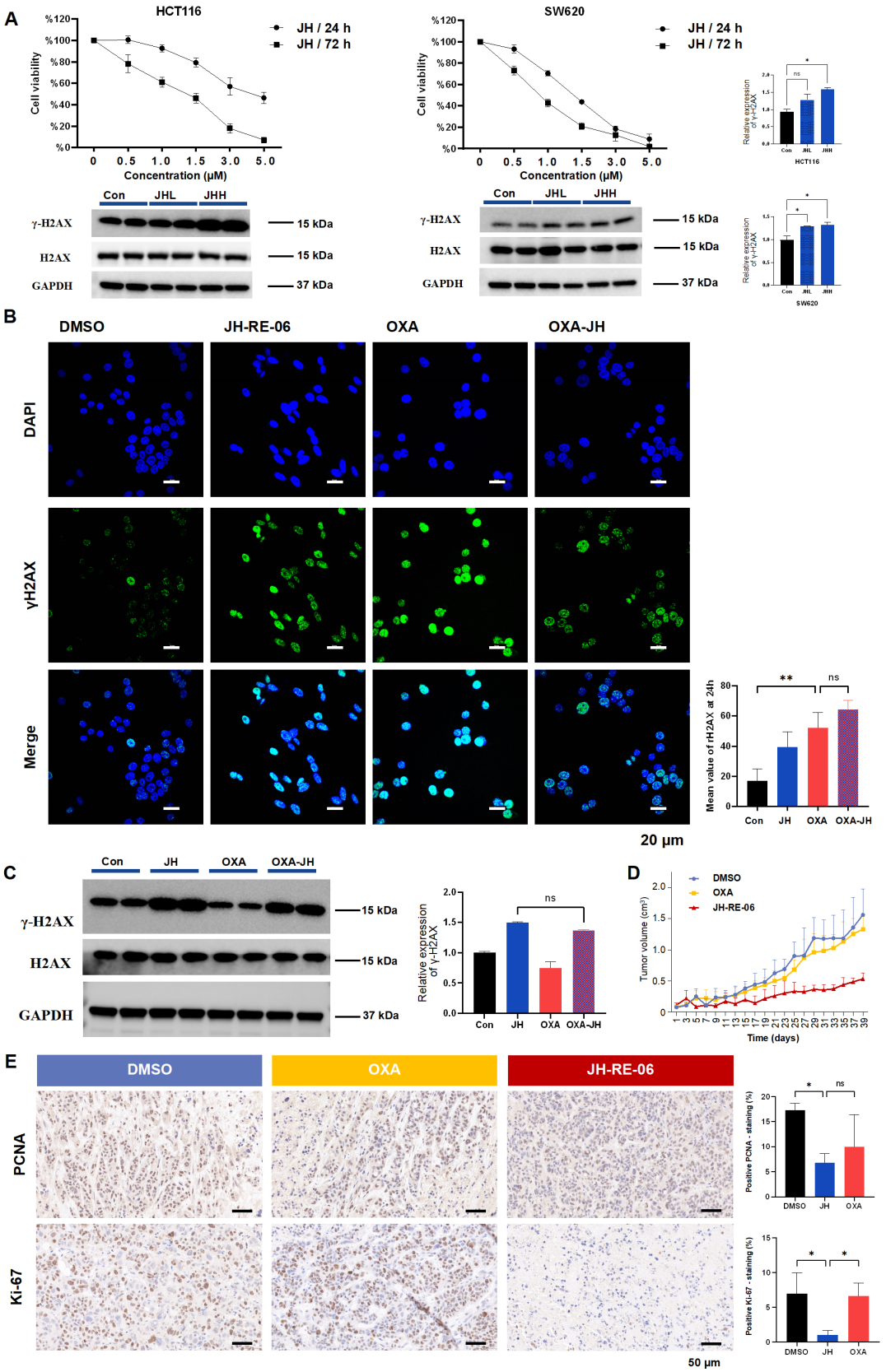

Figure 2. JH, a REV1 DNA directed polymerase inhibitor, suppresses CRC tumorigenesis both *in vitro* and *in vivo*. (A) Cell viability assessed by Cell Counting Kit-8 revealed differential sensitivity to JH, with sustained effects observed at 72 h vs. 24 h in CRC models. WB analysis was used to detect γH2AX levels in cells treated with JH for 24 h. For HCT116 cells, JHL represents 1.5 and JHH represents 3.0 μM JH. For SW620 cells, JHL represents 1.0 and JHH represents 1.5 μM JH. Concentrations were selected based on treatments that resulted in ~50% cell viability after 24 or 72 h. GAPDH was used as the internal control. (B) Immunofluorescence staining of γH2AX in HCT116 cells treated with 3.0 μM JH and/or 5.0 μM OXA for 12 and 24 h. Scale bar, 20 μm. (C) WB analysis of γH2AX levels after treatment with JH and/or OXA, with GAPDH as the loading control. Quantitative analysis revealed no significant differences between the JH and OXA-JH treatment groups. (D) Tumor growth curves for OXA-resistant HCT116 cell xenografts in mice. (E) Representative immunohistochemical images of PCNA and Ki-67 staining in tumor sections. Scale bar, 50 μm. **P<0.01, *P<0.05. CRC, colorectal cancer; JHH, JH-RE-06 high; JHL, JH-RE-06 low; WB, western blot; H2AX, histone H2AX; OXA, oxaliplatin; PCNA, proliferating cell nuclear antigen; Con, control; ns, not significant.

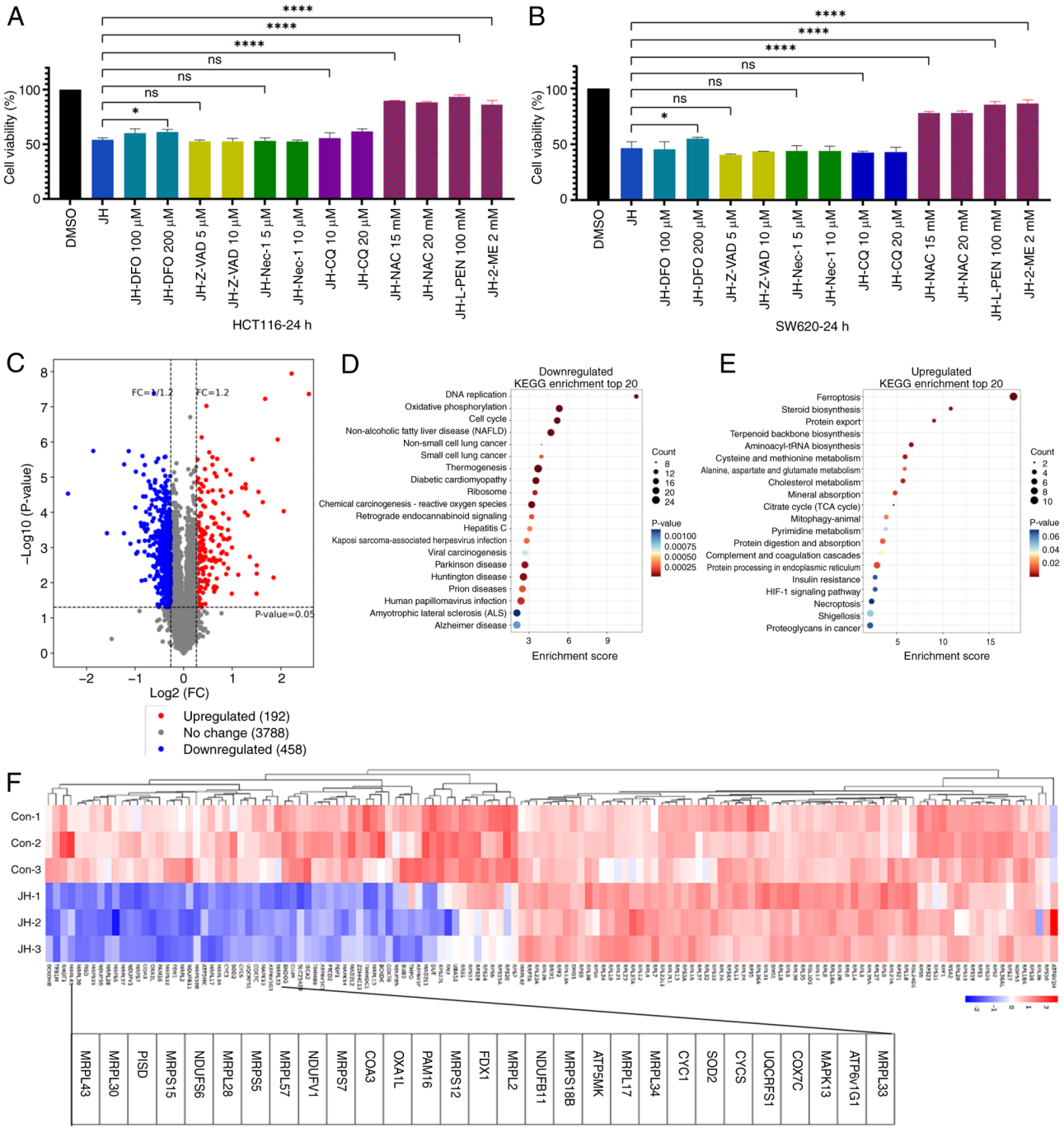

Figure 3. Cell death induced by REV1 DNA directed polymerase inhibition is associated with oxidative stress and ferroptosis. Viability of (A) HCT116 cells treated with 3 μM JH and (B) SW620 cells treated with 1.5 μM JH in the presence or absence of inhibitors. (C) Differentially expressed proteins enriched by proteomics. Compared with the DMSO group, JH upregulated 192 proteins and downregulated 458 proteins. (D) Downregulated pathways. The top 20 enriched KEGG pathways are illustrated. (E) Upregulated pathways. (F) Hierarchical clustering of differentially expressed mitochondrial-associated genes. ****P<0.0001, *P<0.05. JH, JH-RE-06; KEGG, Kyoto encyclopedia of genes and genomes; DFO, deferoxamine; Z-VAD, z-vad-fmk; Nec, necrostatin-1; CQ, chloroquine; NAC, n-acetylcysteine; L-PEN, l-penicillamine; ME, 2-mercaptoethanol; ns, not significant; Con, control; FC, fold change; MRPL, mitochondrial ribosomal protein large subunit; MRPS, mitochondrial ribosomal protein small subunit; NDUF, NADH:ubiquinone oxidoreductase subunit.

with 3.0 μM JH-RE-06. This decrease was consistent with proteomics findings (Fig. 4E). Taken together, these results suggest that JH-RE-06 triggered ferroptosis in CRC cells.

JH-RE-06 triggers ferroptosis via NCOA4-mediated ferritinophagy in CRC cells. Ferroptosis represents an iron-catalyzed, lipid peroxidation-mediated programmed cell death pathway (22). NCOA4-mediated ferritinophagy plays a critical role in ferroptosis by regulating cellular iron homeostasis (23). Ferritinophagy, the autophagic degradation of ferritin, increases the LIP, which promotes ferroptosis (24). CRC cells are both iron-rich and iron-dependent (25), making the regulation of iron homeostasis a key factor in CRC progression and therapeutic resistance (26). Proteomics sequencing revealed elevated NCOA4 expression and a decrease in its regulatory proteins, suggesting that NCOA4 is key for modulating

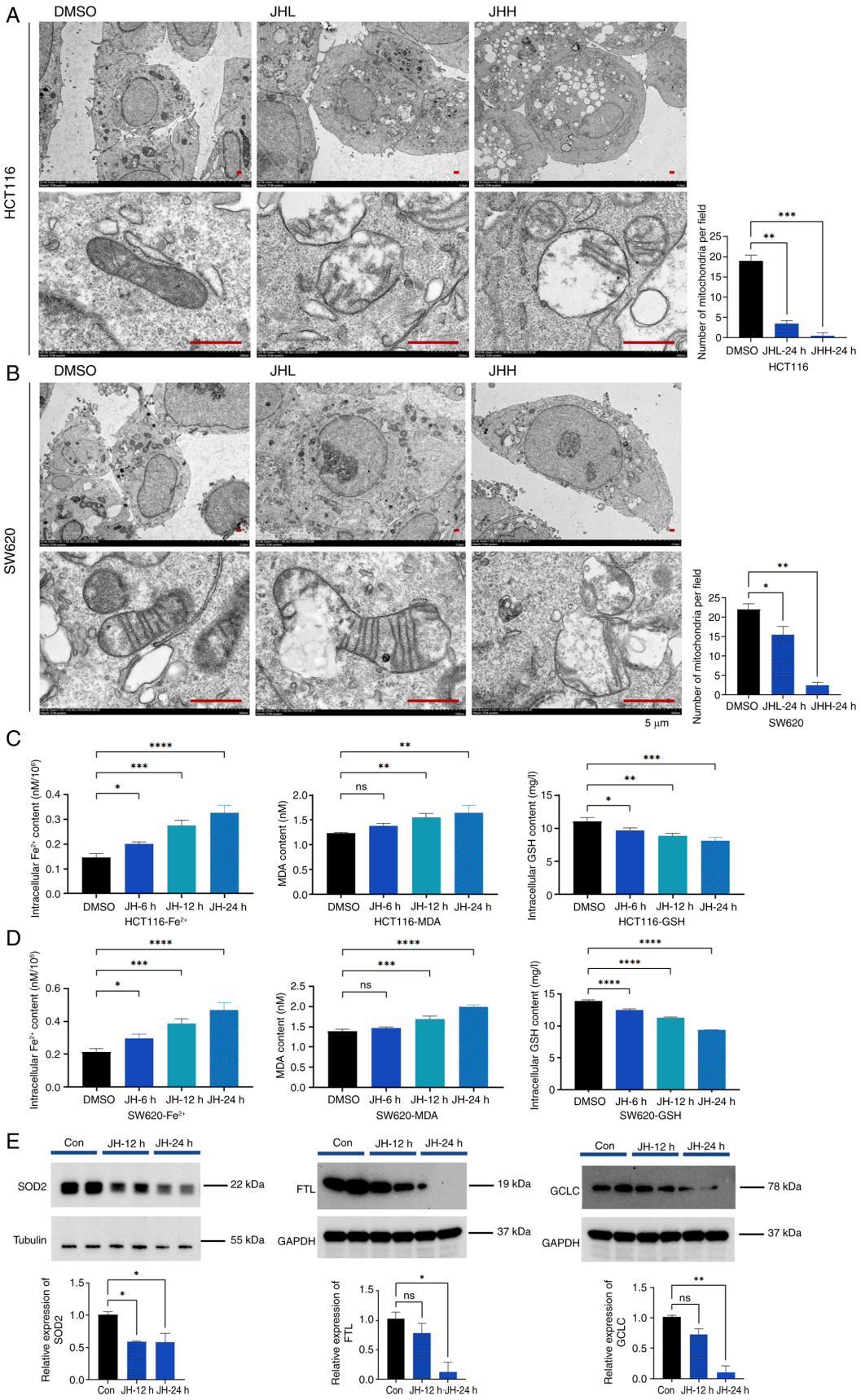

Figure 4. JH triggers ferroptosis in colorectal cancer cells. Transmission electron microscopy of (A) HCT116 and (B) SW620 cells treated with JHL and JHH for 24 h show intracellular vacuolar changes, with mitochondria-like structures undergoing digestion inside the vacuoles. Scale bar, 5 μm. Changes in intracellular Fe^{2+} concentration, MDA and GSH levels (normalized to total protein) in (C) HCT116 cells treated with 3.0 μM JH and (D) SW620 cells treated with 1.5 μM JH at 6, 12 and 24 h post-treatment. (E) Relative protein expression levels of SOD2, FTL and GCLC following 12 and 24 h JH treatment in HCT116 cells; 24 h exposure to JH resulted in significant downregulation of antioxidant proteins SOD2, FTL and GCLC. ****P<0.0001, ***P<0.001, **P<0.01, *P<0.05. JHH, JH-RE-06 high; JHL, JH-RE-06 low; MDA, malondialdehyde; GSH, glutathione; SOD2, superoxide dismutase 2; FTL, ferritin light chain; GCLC, glutamate-cysteine ligase catalytic subunit; ns, not significant; Con, control.

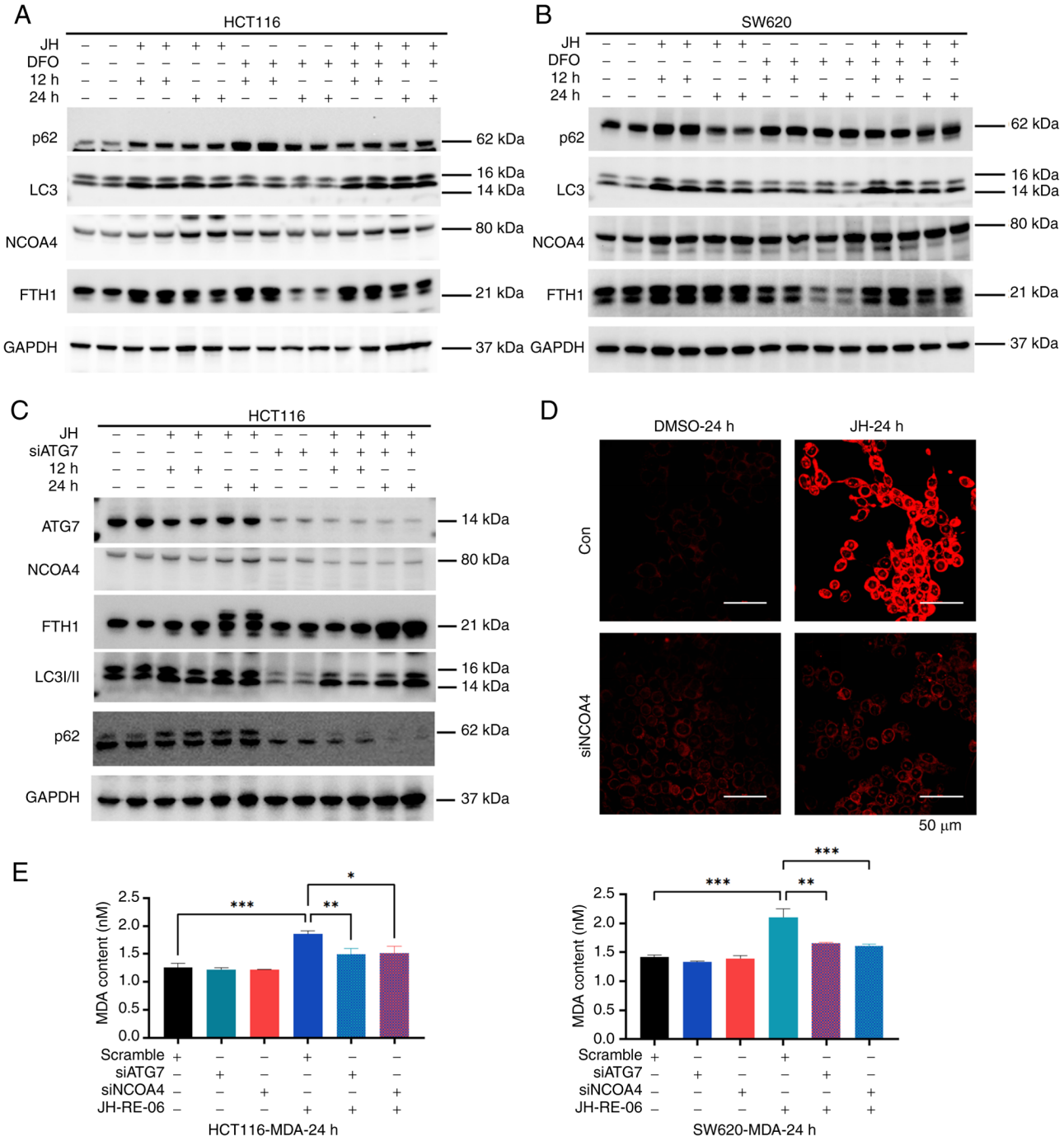

Figure 5. JH triggers ferroptosis via NCOA4-mediated ferritinophagy in colorectal cancer cells. (A) HCT116 cells were treated with 3.0 μM JH and (B) SW620 cells with 1.5 μM JH and/or 50 μM DFO for 12 and 24 h before WB analysis for p62, LC3, NCOA4 and FTH1, normalized to GAPDH. (C) WB analysis of HCT116 cells with or without ATG7 knockout, treated with 3.0 μM JH. (D) HCT116 cells were transfected with scramble or siNCOA4 for 48 h, then treated with 3.0 μM JH for 24 h. Cells were incubated with FerroOrange probe and imaged using laser confocal microscopy. Scale bar, 50 μm. (E) Lipid peroxidation levels were measured in ATG7 and NCOA4 knockdown cells, as well as wild-type HCT116 and SW620 cells, treated with JH. ***P<0.001, **P<0.01, *P<0.05. JH, JH-RE-06; NCOA4, nuclear receptor coactivator 4; WB, western blot; LC3, microtubule-associated protein 1 light chain 3; FTH, ferritin heavy chain; ATG, autophagy-related gene; si, small interfering; DFO, deferoxamine.

cellular iron levels following JH-RE-06 treatment. Therefore, it was hypothesized that JH-RE-06 increased the LIP in an NCOA4-dependent manner, thereby inducing ferroptosis via ferritinophagy. To validate this hypothesis, the present study assessed changes in the expression of ferritinophagy-associated proteins following JH-RE-06 treatment in CRC cells using western blotting. JH-RE-06 increased the expression of NCOA4, p62 and LC3 at both 12 and 24 h (Figs. 5A and B and S2B and C). FTH1 expression increased at 12 but decreased by 24 h. To verify the reliability of the experimental system, DFO was used to chelate Fe^{2+} and protein levels of LC3II, NCOA4, and p62 were increased (Figs. 5A and B). Next, the role of LIP in mediating the effects of JH-RE-06 was explored by pre-treating cells with DFO to chelate Fe^{2+}, followed by JH-RE-06 treatment. In the combination group, NCOA4 expression was sustained for longer period with the DFO

group, and FTH1 levels were also elevated. To investigate the role of ferritinophagy, ATG7 or NCOA4, key proteins involved in ferritinophagy and Fe^{2+} recycling, were silenced before treating the cells with JH-RE-06 (Fig. S2D). In these cells, the expression of NCOA4, LC3II, and p62 in response to JH-RE-06 was partially mitigated (Figs. 5C and S2D), and FTH1, a substrate for ferritinophagy degradation, accumulated due to impaired autophagy (Fig. 4C and S2E). LIP was assessed using the FerroOrange test. In wild-type HCT116 cells, JH-RE-06 treatment induced a significant increase in LIP at 24 h, indicating iron overload. However, in siNCOA4 cells, the JH-RE-06-induced increase in LIP was not observed at 24 h due to the inhibition of ferritin degradation. This suggested that the iron overload induced by JH-RE-06 is dependent on functional NCOA4-mediated ferritinophagy (Fig. 5D). Silencing ATG7 or NCOA4 before JH-RE-06 treatment resulted in decreased MDA levels (Fig. 5E). Based on these findings, it was hypothesized that JH-RE-06 induces ferroptosis through NCOA4-mediated ferritinophagy, disrupting iron homeostasis and promoting lipid peroxidation.

Discussion

REV1 is implicated in cancer development by enabling cells to bypass DNA damage, thereby accumulating genetic mutations and increasing cancer risk (14). Most CRCs originate from polyps, which progress through abnormal crypts into neoplastic precursor lesions over 10-15 years (27). The present study highlighted the clinical value of REV1 in CRC. Bioinformatics analysis and immunohistochemical staining of tissue microarrays revealed that high tumoral REV1 expression served as a negative prognostic indicator. Furthermore, bioinformatics analysis identified a significant association between high REV1 expression and the presence of colon polyps, indicating its potential role in early colorectal tumorigenesis. These findings collectively suggested that REV1 is a promising therapeutic target for both early intervention and advanced CRC treatment.

Studies have focused on enhancing cancer cell sensitivity to platinum-based agents by genetically inhibiting REV1 (6,7). Early studies proposed that REV1 ablation may potentiate OXA efficacy by exacerbating DNA damage and apoptosis (21,28). However, OXA primarily exerts cytotoxic effects via ribosome biogenesis stress, independent of DNA damage mechanisms (29). Similarly, the present study revealed that pretreatment with the REV1 inhibitor JH-RE-06 enhanced cellular resistance to OXA or oncogene-induced (cyclin E overexpression) RS can render cancer cells hypersensitive to TLS inhibition (11,30). Clinically, while OXA treatment often leads to drug resistance in CRC, it generates a therapeutic vulnerability that may be exploited (31). To validate this hypothesis, the present study established OXR CRC models. Both clonogenic assays and xenograft experiments revealed that JH-RE-06 selectively inhibited OXR cell proliferation while exhibiting minimal toxicity, positioning it as a promising second-line therapeutic candidate for refractory CRC.

While previous research has explored the effects of JH-RE-06 in lung and BRCA1/2-deficient cancer (10,18), the specific PCD mechanisms remain unclear. The present study established JH-RE-06 as a DNA-damaging agent that inhibited CRC cell proliferation in a dose-dependent manner. Pharmacological rescue experiments revealed that JH-RE-06-induced cell death was mitigated by cysteine regenerators (L-penicillamine, 2-mercaptoethanol and N-acetylcysteine) and the iron chelator DFO, suggesting that the cell death mechanism was consistent with ferroptosis rather than conventional PCD pathways such as apoptosis, necrosis or autophagy. Ferroptosis is a metabolically regulated cell death process driven by iron-dependent lipid peroxidation and compromised redox balance (32). In the present study, proteomics analysis confirmed that JH-RE-06 promoted cell signaling pathways associated with 'DNA replication', 'ferroptosis', and 'oxidative phosphorylation'.

JH-RE-06 treatment in CRC cells resulted in decreased mitochondrial abundance and intracellular GSH levels, and significant elevations in intracellular Fe^{2+} and MDA concentrations, which represent key features of ferroptosis. Consistent with these findings, REV1 deficiency-induced RS causes metabolic stress, leading to mitochondrial dysfunction in mouse embryonic fibroblasts (33). Studies in $REV1^{-/-}$ mice (a replication stress model) (21) have demonstrated sex-dependent metabolic disturbances, underscoring the dual role of REV1 in DNA stability and metabolic control (34).

The association between REV1 inhibition and ferroptosis remains incompletely understood. However, emerging evidence indicates NCOA4-mediated ferritinophagy as a key mechanism, involving iron liberation through ferritin degradation and RS via minichromosome maintenance protein complex 2-7, helicase interference (35). JH-RE-06 treatment in wild-type CRC cells significantly upregulated both autophagy markers (LC3I/II and p62) and ferritinophagy-associated proteins. This was characterized by increased NCOA4 expression, decreased FTH1 levels and consequent elevation of LIP. The experimental system was validated by using DFO to chelate Fe^{2+}, which demonstrated target protein changes aligned with prior reports (36,37). By contrast, ATG7 knockout CRC cells exhibited increased FTH1 levels and no increase in LIP following JH-RE-06 treatment. Moreover, JH-RE-06-treated autophagy-deficient CRC cells showed decreased MDA levels, indicating that the ferroptosis induced by JH-RE-06 may depend on NCOA4-mediated ferritinophagy. Recent research has highlighted the role of NCOA4 in regulating both DNA replication origins and iron autophagy-mediated LIP, with potential Fe-S cluster degradation (38). REV1 protects replication forks by suppressing their remodeling (11), while NCOA4 regulates DNA replication origins, preventing RS (39). However, the precise regulatory association between REV1 inhibition and NCOA4 remains to be fully elucidated.

Recent studies have indicated the potential of REV1 inhibitors as regulators of cell metabolism for cancer therapy (40,41). In epithelial ovarian cancer, fumarate-mediated modulation of TLS may enhance the efficacy of genotoxic chemotherapy (40). In pulmonary malignancy, REV1 promotes radioresistance by modulating amino acid metabolism, specifically via cystathionine γ-lyase ubiquitination and subsequent disruption of Gly/Ser/Thr metabolic flux (41). These findings suggest that the development of more selective REV1 inhibitors may offer novel therapeutic opportunities, especially when conventional apoptosis mechanisms are compromised.

The present findings established REV1 as both a prognostic marker and therapeutic candidate in CRC, with elevated expression associated with poorer survival. The specific inhibitor JH-RE-06 induced DNA damage and suppressed tumor cell proliferation, while also triggering oxidative stress in CRC cells. JH-RE-06 regulated intracellular iron overload via NCOA4-mediated ferritinophagy, thereby activating ferroptosis. This led to an increase in the LIP, contributing to oxidative stress and initiating ferroptosis, which was reversed by DFO and free radical scavengers such as NAC. JH-RE-06 effectively inhibited the proliferation of CRC cells, highlighting its clinical potential as a therapeutic option for CRC, including both treatment-naive and chemotherapy-resistant forms.

Acknowledgements

Not applicable.

Funding

The present study was supported by the Ningxia Hui Autonomous Region Science and Technology Support Program (grant no. 2021BEG03084) and the Ningxia Education Department's Scientific Research Program (grant no. NYG2024117).

Availability of data and materials

The data generated in the present study may be found in the Open Archive for Miscellaneous Data, China National Center for Bioinformation under accession number OMIX007702 or at the following URL: ngdc.cncb.ac.cn/omix/release/OMIX007702.

Authors' contributions

JC conceived and designed the study, performed experiments, analyzed data and wrote the manuscript. XY, WZ and JX performed experiments. FX conceived the study, revised the manuscript for important intellectual content, and assisted in the interpretation of key experimental results. XY revised the manuscript and participated in data analysis. JC and XY confirm the authenticity of all the raw data. YH participated in key experimental operations (optimization of ROS detection protocols, paraffin sectioning techniques, as applicable) and verification of experimental protocols. All authors have read and approved the final manuscript.

Ethics approval and consent to participate

All procedures adhered to institutional guidelines and received approval from the Ethics Committee of Ningxia Medical University Laboratory Animal Center (approval no. IACUC-NYLAC-2022-022), in compliance with the ARRIVE guidelines and national regulations for humane treatment of animals. The human tissue microarrays were commercially sourced from fully de-identified samples previously collected under ethical oversight. In accordance with international research standards (Declaration of Helsinki) and institutional policies for the secondary use of archival specimens, no additional ethical review or consent procedures were required.

Patient consent for publication

Not applicable.

Competing interests

The authors declare that they have no competing interests.

References

1. Sung H, Ferlay J, Siegel RL, Laversanne M, Soerjomataram I, Jemal A and Bray F: Global cancer statistics 2020: GLOBOCAN estimates of incidence and mortality worldwide for 36 cancers in 185 countries. CA Cancer J Clin 71: 209-249, 2021.
2. Liu Z, Xu Y, Xu G, Baklaushev VP, Chekhonin VP, Peltzer K, Ma W, Wang X, Wang G and Zhang C: Nomogram for predicting overall survival in colorectal cancer with distant metastasis. BMC Gastroenterol 21: 103, 2021.
3. Veenstra CM and Krauss JC: Emerging systemic therapies for colorectal cancer. Clin Colon Rectal Surg 31: 179-191, 2018.
4. Berti M, Cortez D and Lopes M: The plasticity of DNA replication forks in response to clinically relevant genotoxic stress. Nat Rev Mol Cell Biol 21:633-651, 2020.
5. Yang W and Gao Y: Translesion and repair DNA polymerases: Diverse structure and mechanism. Annu Rev Biochem 87: 239-261, 2018.
6. Hicks JK, Chute CL, Paulsen MT, Ragland RL, Howlett NG, Gueranger Q, Glover TW and Canman CE: Differential roles for DNA polymerases eta, zeta, and REV1 in lesion bypass of intrastrand versus interstrand DNA cross-links. Mol Cell Biol 30: 1217-1230, 2010.
7. Sharma S, Hicks JK, Chute CL, Brennan JR, Ahn JY, Glover TW and Canman CE: REV1 and polymerase ζ facilitate homologous recombination repair. Nucleic Acids Res 40: 682-691, 2012.
8. Baranovskiy AG, Lada AG, Siebler HM, Zhang Y, Pavlov YI and Tahirov TH: DNA polymerase delta and zeta switch by sharing accessory subunits of DNA polymerase delta. J Biol Chem 287: 17281-17287, 2012.
9. Mellor C, Nassar J, Šviković S and Sale JE: PRIMPOL ensures robust handoff between on-the-fly and post-replicative DNA lesion bypass. Nucleic Acids Res 52: 243-258, 2024.
10. Taglialatela A, Leuzzi G, Sannino V, Cuella-Martin R, Huang JW, Wu-Baer F, Baer R, Costanzo V and Ciccia A: REV1-Polzeta maintains the viability of homologous recombination-deficient cancer cells through mutagenic repair of PRIMPOL-dependent ssDNA gaps. Mol Cell 81: 4008-4025 e7, 2021.
11. Nayak S, Calvo JA, Cong K, Peng M, Berthiaume E, Jackson J, Zaino AM, Vindigni A, Hadden MK and Cantor SB: Inhibition of the translesion synthesis polymerase REV1 exploits replication gaps as a cancer vulnerability. Sci Adv 6: eaaz7808, 2020.
12. Nayak S, Calvo JA and Cantor SB: Targeting translesion synthesis (TLS) to expose replication gaps, a unique cancer vulnerability. Expert Opin Ther Targets 25: 27-36, 2021.
13. Lin X and Howell SB: DNA mismatch repair and p53 function are major determinants of the rate of development of cisplatin resistance. Mol Cancer Ther 5: 1239-1247, 2006.
14. Sasatani M, Xi Y, Kajimura J, Kawamura T, Piao J, Masuda Y, Honda H, Kubo K, Mikamoto T, Watanabe H, *et al*: Overexpression of Rev1 promotes the development of carcinogen-induced intestinal adenomas via accumulation of point mutation and suppression of apoptosis proportionally to the Rev1 expression level. Carcinogenesis 38: 570-578, 2017.
15. Zhu N, Zhao Y, Mi M, Lu Y, Tan Y, Fang X, Weng S and Yuan Y: REV1: A novel biomarker and potential therapeutic target for various cancers. Front Genet 13: 997970, 2022.
16. Wojtaszek JL, Chatterjee N, Najeeb J, Ramos A, Lee M, Bian K, Xue JY, Fenton BA, Park H, Li D, *et al*: A small molecule targeting mutagenic translesion synthesis improves chemotherapy. Cell 178: 152-159.e11, 2019.

17. Chatterjee N, Whitman MA, Harris CA, Min SM, Jonas O, Lien EC, Luengo A, Vander Heiden MG, Hong J, Zhou P, *et al*: REV1 inhibitor JH-RE-06 enhances tumor cell response to chemotherapy by triggering senescence hallmarks. Proc Natl Acad Sci USA 117: 28918-28921, 2020.
18. Chen Y, Jie X, Xing B, Wu Z, Yang X, Rao X, Xu Y, Zhou D, Dong X, Zhang T, *et al*: REV1 promotes lung tumorigenesis by activating the Rad18/SERTAD2 axis. Cell Death Dis 13: 110, 2022.
19. Dobin A, Davis CA, Schlesinger F, Drenkow J, Zaleski C, Jha S, Batut P, Chaisson M and Gingeras TR: STAR: Ultrafast universal RNA-seq aligner. Bioinformatics 29: 15-21, 2013.
20. Mizuno H, Kitada K, Nakai K and Sarai A: PrognoScan: A new database for meta-analysis of the prognostic value of genes. BMC Med Genomics 2: 18, 2009.
21. Sharma S, Shah NA, Joiner AM, Roberts KH and Canman CE: DNA polymerase ζ is a major determinant of resistance to platinum-based chemotherapeutic agents. Mol Pharmacol 81: 778-787, 2012.
22. Dixon SJ, Lemberg KM, Lamprecht MR, Skouta R, Zaitsev EM, Gleason CE, Patel DN, Bauer AJ, Cantley AM, Yang WS, *et al*: Ferroptosis: An iron-dependent form of nonapoptotic cell death. Cell 149: 1060-1072, 2012.
23. Gao M, Monian P, Pan Q, Zhang W, Xiang J and Jiang X: Ferroptosis is an autophagic cell death process. Cell Res 26: 1021-1032, 2016.
24. Hou W, Xie Y, Song X, Sun X, Lotze MT, Zeh HJ III, Kang R and Tang D: Autophagy promotes ferroptosis by degradation of ferritin. Autophagy 12: 1425-1428, 2016.
25. Radulescu S, Brookes MJ, Salgueiro P, Ridgway RA, McGhee E, Anderson K, Ford SJ, Stones DH, Iqbal TH, Tselepis C and Sansom OJ: Luminal iron levels govern intestinal tumorigenesis after Apc loss in vivo. Cell Rep 2: 270-282, 2012.
26. Hu Q, Wei W, Wu D, Huang F, Li M, Li W, Yin J, Peng Y, Lu Y, Zhao Q and Liu L: Blockade of GCH1/BH4 axis activates ferritinophagy to mitigate the resistance of colorectal cancer to erastin-induced ferroptosis. Front Cell Dev Biol 10: 810327, 2022.
27. Dekker E, Tanis PJ, Vleugels JLA, Kasi PM and Wallace MB: Colorectal cancer. Lancet 394: 1467-1480, 2019.
28. Xie K, Doles J, Hemann MT and Walker GC: Error-prone translesion synthesis mediates acquired chemoresistance. Proc Natl Acad Sci USA 107: 20792-20797, 2010.
29. Bruno PM, Liu Y, Park GY, Murai J, Koch CE, Eisen TJ, Pritchard JR, Pommier Y, Lippard SJ and Hemann MT: A subset of platinum-containing chemotherapeutic agents kills cells by inducing ribosome biogenesis stress. Nat Med 23: 461-471, 2017.
30. Sekimoto T, Oda T, Kurashima K, Hanaoka F and Yamashita T: Both high-fidelity replicative and low-fidelity Y-family polymerases are involved in DNA rereplication. Mol Cell Biol 35: 699-715, 2015.
31. Wang G, Wang JJ, Zhi-Min Z, Xu XN, Shi F and Fu XL: Targeting critical pathways in ferroptosis and enhancing antitumor therapy of Platinum drugs for colorectal cancer. Sci Prog 106: 368504221147173, 2023.
32. Jiang X, Stockwell BR and Conrad M: Ferroptosis: Mechanisms, biology and role in disease. Nat Rev Mol Cell Biol 22: 266-282, 2021.
33. Fakouri NB, Durhuus JA, Regnell CE, Angleys M, Desler C, Hasan-Olive MM, Martín-Pardillos A, Tsaalbi-Shtylik A, Thomsen K, Lauritzen M, *et al*: Rev1 contributes to proper mitochondrial function via the PARP-NAD+-SIRT1-PGC1alpha axis. Sci Rep 7: 12480, 2017.
34. Anugula S, Li Z, Li Y, Hendriksen A, Christensen PB, Wang L, Monk JM, de Wind N, Bohr VA, Desler C, *et al*: Rev1 deficiency induces a metabolic shift in MEFs that can be manipulated by the NAD(+) precursor nicotinamide riboside. Heliyon 9: e17392, 2023.
35. Federico G, Carrillo F, Dapporto F, Chiariello M, Santoro M, Bellelli R and Carlomagno F: NCOA4 links iron bioavailability to DNA metabolism. Cell Rep 40: 111207, 2022.
36. Wu H, Liu Q, Shan X, Gao W and Chen Q: ATM orchestrates ferritinophagy and ferroptosis by phosphorylating NCOA4. Autophagy 19: 2062-2077, 2023.
37. Zhang MJ, Song ML, Zhang Y, Yang XM, Lin HS, Chen WC, Zhong XD, He CY, Li T, Liu Y, *et al*: SNS alleviates depression-like behaviors in CUMS mice by regluating dendritic spines via NCOA4-mediated ferritinophagy. J Ethnopharmacol 312: 116360, 2023.
38. Kuno S and Iwai K: Oxygen modulates iron homeostasis by switching iron sensing of NCOA4. J Biol Chem 299: 104701, 2023.
39. Bellelli R, Castellone MD, Guida T, Limongello R, Dathan NA, Merolla F, Cirafici AM, Affuso A, Masai H, Costanzo V, *et al*: NCOA4 transcriptional coactivator inhibits activation of DNA replication origins. Mol Cell 55: 123-137, 2014.
40. Li J, Zheng C, Mai Q, Huang X, Pan W, Lu J, Chen Z, Zhang S, Zhang C, Huang H, *et al*: Tyrosine catabolism enhances genotoxic chemotherapy by suppressing translesion DNA synthesis in epithelial ovarian cancer. Cell Metab 35: 2044-2059.e8, 2023.
41. Chen Y, Feng X, Wu Z, Yang Y, Rao X, Meng R, Zhang S, Dong X, Xu S, Wu G and Jie X: USP9X-mediated REV1 deubiquitination promotes lung cancer radioresistance via the action of REV1 as a Rad18 molecular scaffold for cystathionine γ-lyase. J Biomed Sci 31: 55, 2024.